Highly efficient inverted circularly polarized organic light emitting diodes

Li Wan[a], Jessica Wade[ab], Xingyuan Shi[ab], Shengda Xu[c], Matthew J. Fuchter[b] and Alasdair J. Campbell[a*]*

[a]Department of Physics and Centre for Processable Electronics, Imperial College London, South Kensington Campus, London SW7 2AZ,UK [b]Department of Chemistry and Molecular Sciences Research Hub, Imperial College London, White City Campus, 80 Wood Lane, London W12 0BZ, UK [c]Department of Materials and Centre for Processable Electronics, Imperial College London, South Kensington Campus, London SW7 2AZ, UK

KEYWORDS circular polarization, chiral materials, light emitting polymers, inverted light emitting diodes, device architecture

ABSTRACT

Circularly polarized (CP) electroluminescence has been demonstrated as a strategy to improve the performance of organic light emitting diode (OLED) displays. CP emission can be generated from both small molecule and polymer OLEDs (SM-OLEDs and PLEDs), but to date, these devices suffer from low dissymmetry factors (g-factor <0.1), poor device performance, or a combination of the two. Here, we demonstrate the first CP-PLED employing an inverted device architecture.

Through this approach, we demonstrate a highly efficient CP-PLED, with a current efficiency (CE) of 16.4 cd/A, a power efficiency (PE) of 16.6 lm/W, a maximum luminance of over 28,500 cd/m^2, and a high EL dissymmetry (g_{EL}) of 0.57. We find that the handedness of the emitted light is sensitive to the PLED device architecture: the sign of CP-EL from an identically prepared active layer reverses between inverted and conventional devices. The inverted structure affords the first demonstration of CP-PLEDs exhibiting *both* high efficiency and high dissymmetry – the two figures of merit which, until now, have been difficult to achieve at the same time. We also highlight device architecture and associated internal electric field to be a previously unexplored means to control the handedness of CP emission. Our findings significantly broaden the versatility of CP emissive devices and should enable their further application in a variety of other CP-dependent technologies.

MANUSCRIPT

INTRODUCTION

State-of-the-art design of organic light-emitting diode (OLED) displays incorporate light extraction layers capped with a circular polarizer to reduce glare and improve contrast. The external quantum efficiency (η_{EQE}) of an OLED device can be described as:

$$\eta_{EQE,Display} = \xi\eta_{EQE,Device} = \xi\gamma\eta_{IQE} \quad (1)$$

where η_{IQE} is the internal quantum efficiency influenced by the photoluminescence quantum efficiency (PLQE, η_{PL}), radiative recombination efficiency and spin statistics, γ is the out-coupling efficiency and ξ refers to the light loss caused by the in-screen circular polarizing filter.[1]

Strategies to improve the first two factors (η_{IQE} and γ) have been well studied *via* (1) molecular design of emitters (including phosphorescent[2] and Thermally Activated Delayed Fluorescence emitters[1]) and (2) matching the refractive indices of all the constituent layers of a device.[3] There has been recent interest in the use of OLEDs which emit circularly polarized (CP) light (CP-OLEDs) as a means to increase display efficiency by minimizing the light loss caused by the integrated circular polarizer.[4–8] The experimental dissymmetry (*g*-factor) of the emitted circularly polarized light (CPL) is defined as: [9]

$$g = \frac{I_L - I_R}{\frac{1}{2}(I_L + I_R)} \tag{2}$$

where subscripts L and R refer to Left-Handed (LH) and Right-Handed (RH) emission, respectively,[4] thus ξ can be derived as a function of *g*:

$$\xi = \frac{1}{2}\left(\frac{1}{2}g + 1\right) \tag{3}$$

Equation 3 indicates that if $g = 2.0$ (full circular polarization), $\xi = 1$, which means that there is no light loss at the circular polarizer, while if $g = 0$ (no circular polarization), $\xi = 0.5$, which means the light intensity decreases by 50%; as is the case for all conventional non-CP OLEDs used in commercial OLED displays.

With the growing interest in CP-OLEDs, several attempts have been made to fabricate devices using either emissive chiral small molecules (SM-OLEDs)[5,6,10–15] or polymers (PLEDs).[16–19] A full comparison of published CP-OLED performance can be found in Table S1 of the Supporting Information (SI). Although optimized CP-SM-OLEDs can achieve high device performance (93 cd/A, Wu *et al*.[13] and 19.52 cd/A, Yan *et al*.[12]), they feature very low dissymmetry, with *g*-factors

(g_{EL}), typically not exceeding 0.1 and being as low as 0.005 (see Table S1 for details). According to Equation 3, a g_{EL} of 0.1 is equivalent to 5% efficiency improvement, regardless of the type of emissive species. Alternatively, given the high dissymmetry of lanthanide CP emission (*g*-factors typically greater than 1), lanthanide complexes have been considered for CP-SM-OLEDs; however, such devices exhibit very low device performance, in part due to the weak emission of lanthanide complexes.[6] Supramolecular self-assembly of light-emitting polymers (LEPs) in the solid state is an emerging approach to amplify the chiroptical effects and provide enhanced g_{EL} in CP-PLEDs.[4,18–20] Following early proof-of-concept studies using LEPs with chiral sidechains,[17,21–23] Di Nuzzo *et al*. recently reported high-dissymmetry CP-PLEDs using a chiral poly(fluorene-*alt*-benzothiadiazole) polymer (c-PFBT, with steady-state $g_{EL} \approx 0.6$),[18] but the devices reported suffer from high turn-on voltages (10V at 1cd/m^2) and poor device performance (maximum PE of 0.07 lm/W). Our group and others have explored the potential to blend device-optimized achiral polymers with chiral small-molecule additives.[4,19,20] Since the first example of a CP-PLED blend system (poly(9,9-dioctylfluorene-*alt*-benzothiadiazole [F8BT] + aza[6]H) in 2013 ($g_{EL} = 0.2$),[4] g_{EL} has been further improved through the use of alternative chiral additives and novel fabrication steps.[19,20] Despite their high g_{EL}, the efficiency of devices based on achiral polymer – chiral additive blends is still far below that of their non-CP counterparts. For example, in F8BT CP-PLEDs with the chiral additive R5011 ($g_{EL} = 1.13$), CE = 4.46 cd/A,[19] or aza[6]H ($g_{EL} = 1.05$) CE = 4.00 cd/A,[20] whereas non-CP emitting neat F8BT devices (with similar thickness) can achieve efficiencies of up to 11.8 cd/A, depending on molecular weight and quality of the material.[20,24–26] To the best our knowledge, whilst there have been reports of efficient small molecule based devices (Table S1), there have been no reports of polymer-based devices that achieves both high g_{EL} and high efficiency.[5,6,10–15]

RESULTS AND DISCUSSION

We have previously demonstrated that a strong chiroptical response can be induced in F8BT using aza[6]H and so selected this polymer blend system for further device optimization.[20] It is evident that new approaches are needed to achieve high-performance CP-PLEDs. Conventional OLED structures with low work function (WF) metal top contacts (e.g. calcium) usually suffer from degradation caused by the permeation of water and oxygen. With air-stable metal-oxide electron injection layers and high work function top anode contacts, inverted PLEDs typically show high stability under ambient conditions[24,27] and extended operational lifetime[28]. We use an inverted device architecture to produce CP-PLEDs with an active layer that contained F8BT with 10 wt% [*M*]-aza[6]H (abbreviated as F8BT + 10%[*M*]) (see Figure 1; The geometries of the measurement are defined in Figure S1). Alongside the demonstration of a high-performance inverted green-emitting CP-PLED (16.4 cd/A, 16.6 lm/W), we discover that the handedness of the emitted light depends on the device architecture. It is worth emphasizing that conventionally, CP emission from CP-OLEDs is fixed according to the stereochemistry of the chiral material used in active layer, with only a few exceptions (Table S2). We believe that this work will allow the development of CP-OLEDs with performances compatible with real-world display technologies, as well as offering new ways to manipulate the sign and magnitude of CP light in device applications.

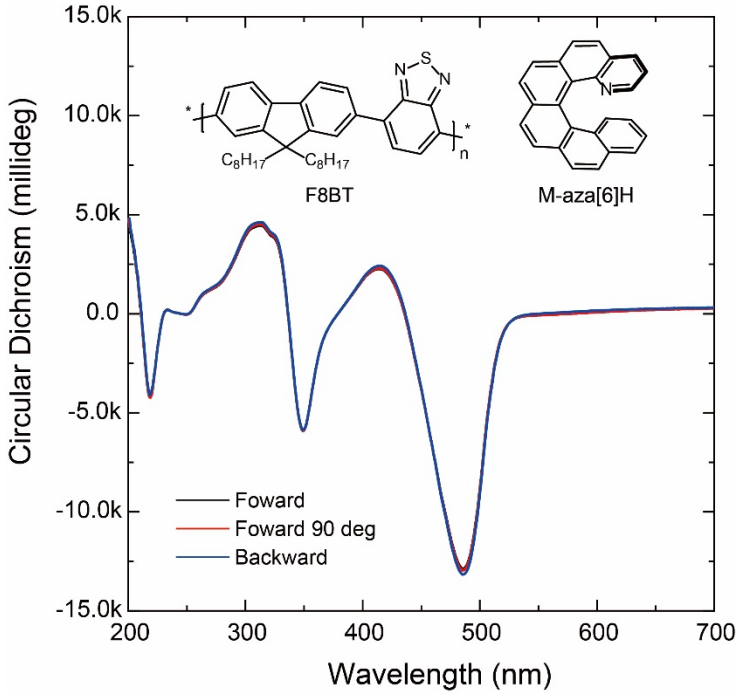

Figure 1. Circular Dichroism spectra of F8BT + 10%[*M*] films. The active layer is deposited after the deposition of PEIE modified ZnO on ITO substrates (see Methods section). Film thickness is 140 nm.

Our inverted devices incorporate PEIE (polyethylenimine ethoxylated; Figure S2) modified ZnO, a solution-processable electron injection layer (EIL)/electron transporting layer (ETL) that is commonly used in inverted OLED device architectures.[27] The WF and morphology of ZnO and PEIE modified ZnO were characterized using Kelvin Probe–Atomic Force Microscope (KP–AFM) measurements (Figure S3). PEIE modified ZnO exhibits a shallower WF (3.75 eV) than neat ZnO (4.36 eV), as the polyamine groups form molecular dipoles that shift the WF.[27,29] PEIE modified ZnO also exhibits a much smoother surface (RMS roughness < 1 nm), which improves the ease of electron injection into the active layer (F8BT LUMO = 3.3 eV). To establish the impact of device architecture on performance, we first fabricated a reference non-CP F8BT (100 nm)

inverted PLED (iPLED) (featuring structure ITO/ZnO(/PEIE)/F8BT(100nm)/MoO_x/Au; Figure S4).

We found this reference device to have comparable performance to devices in prior iPLED studies; with a CE of 6.22 cd/A and maximum luminance = 27,100 cd/m^2.[24,27] To achieve CP emission, multi-layer device stacks with achiral polymer – chiral small molecule additive blend active layers (ITO/ ZnO/ PEIE / F8BT + 10%[*M*]/ MoO_x/ Au) were fabricated. To induce chirality within the active layer, the devices were annealed (140 °C, 10 minutes) in a nitrogen-filled glovebox.[20] Under such temperature, the racemization of aza[6]H is negligible (ΔG = 32.2 kcal/mol, $t_{1/2,\ 140\ °C}$ = ~ 2.4h).[30] Consistent with our previous studies, these films show significant circular dichroism (CD ≈ 14,800 mdeg, thickness = 180 nm, g_{abs} = –1.05) and no obvious changes when flipping or rotating the sample (Figure 1), suggesting no contribution from linear dichroism (LD) or linear birefringence (LB).[20,31,32] It is also noteworthy that this result agrees with Mueller matrix spectroscopic ellipsometry (Figure S17 of Ref[20]), which reveal no linear terms in transmission or reflection. Unfortunately, the inverted CP-PLEDs (iCP-PLEDs) using this device architecture (ITO/ ZnO/ PEIE / F8BT + 10%[*M*]/ MoO_x/ Au) do not achieve the same device performance as the non-CP iPLEDs (Figure S4, Table S3).

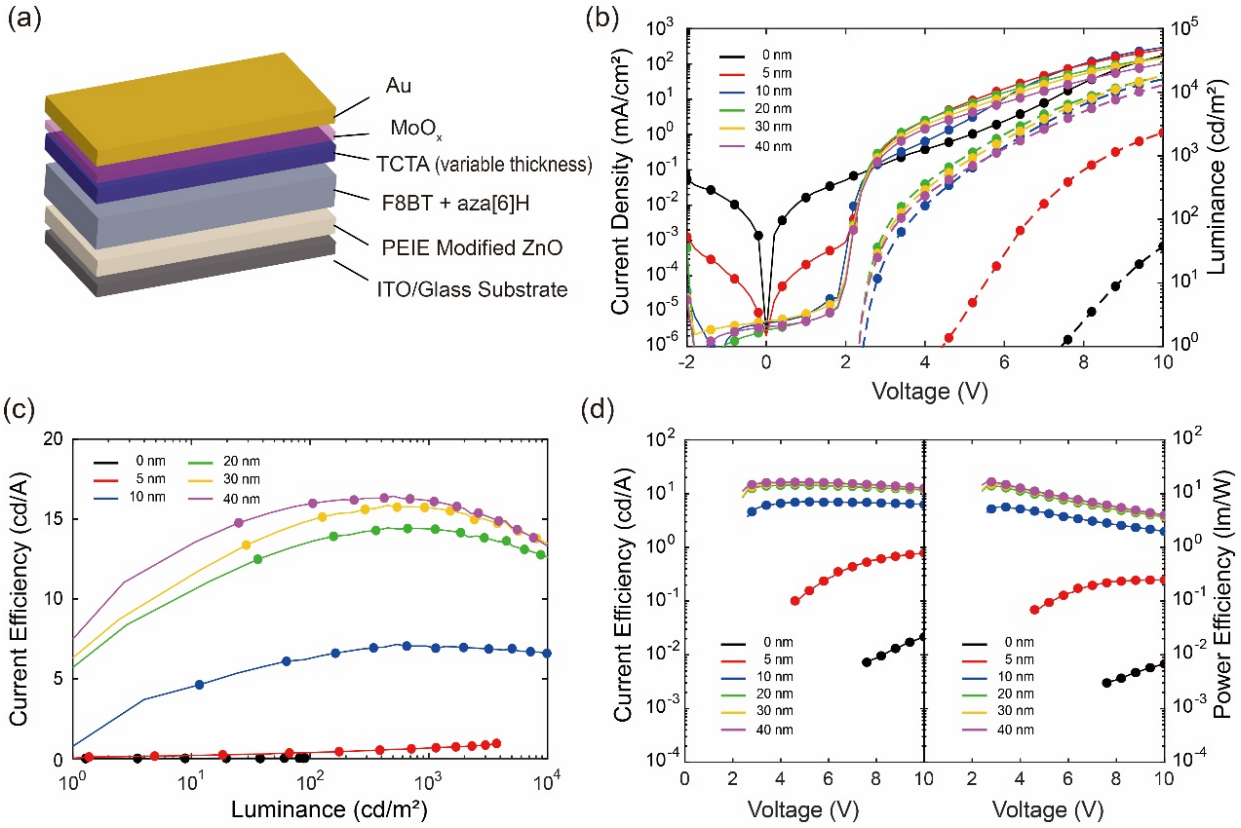

Figure 2. **(a)** Device architecture of the iCP-PLED; **(b)** *J-V-L* curves of the iCP-PLED with varying thicknesses of TCTA interlayer; **(c)** Extracted currency efficiency – luminance curve of **(b)**; **(d)** Extracted current efficiency (CE) and power efficiency (PE) of **(b)** as a function of driving voltage.

To improve the performance of iCP-PLED devices, we investigated the use of a low-cost sublimable hole transport layer (HTL) 4,4',4"-Tris(carbazol-9-yl)triphenylamine (TCTA; Figure S2).[33] As evident from Figure 2, the thickness of the TCTA layer has a marked impact on device performance. An active layer thickness of 180 nm was chosen as it demonstrates an excellent CD signal (Figure 1), as explored in our previous study.[20] The shape of the electroluminescence (EL) spectrum can be impacted by the interlayer thickness in bilayer PLEDs due to the associated change in reflectance, overall device optics and position of the recombination zone (RZ).[34] To

minimize these changes, we investigated the device performance of CP-PLEDs with 5 – 40 nm TCTA HTL (ZnO/PEIE/F8BT+10%[*M*] (180 nm)/TCTA (of variable thickness)/MoO_x/Au; Figure S5). The thickness range was chosen in order to maintain the EL shape of devices and simplify the device optics involved in CP-PLED. (Figure S5) The device performance significantly improves when the TCTA thickness is increased from 5 to 40 nm (Table S4, CE from 0.02 cd/A to 16.4 cd/A, PE from 0.006 lm/W to 16.6 lm/W and maximum luminance from 192 cd/m^2 to 28,500 cd/m^2), while the turn-on voltage decreases (from 7.4 to 2.3 V). It is interesting to note that with 40 nm TCTA the efficiency roll-off is very low – CE only decreases by 9.4% at 3,000 cd/m^2, 16.5% at 5,000 cd/m^2 and 21.3% at 10,000 cd/m^2. As the induced chiroptical response in LEP-chiral small-molecule films is known to be particularly sensitive to the morphology of the active layer,[35] we compared Raman (Figure S6) and CD (Figure S7) spectra of F8BT + 10%[*M*] / TCTA films, where the thickness of the TCTA layer was varied between 5 and 40 nm. The Raman spectrum of F8BT contains vibrational modes corresponding to the symmetric stretching of the aromatic rings in the F8 (9,9-dioctylfluorene, 1609 cm^{-1}) and BT (benzothiadiazole, 1545 cm^{-1}) units.[36] Relative intensities of the BT and F8 Raman modes can be used to estimate inter-unit torsion,[20,36] and are unchanged by the presence of the TCTA layer on top (Figure S6). Similarly, increasing the thickness of TCTA does not impact the intensity or position of the CD peak at $\lambda = 490$ nm. Although the Cotton band at $\lambda \approx 525$ nm is enhanced by 40 nm TCTA (Figure S7), we do not expect this to significantly impact the emission, as the absorption of the active layer at $\lambda = 525$ nm is minimal. Whilst TCTA has no obvious impact on the thin-film morphology of F8BT + 10%[*M*], devices incorporating 40 nm TCTA show dramatically enhanced g_{EL} from 0.04 (without TCTA) to 0.57 (see Figure S8 for detailed CP-EL spectra). We attribute this increase in g_{EL} to the movement of the RZ within the active layer; as the RZ shifts away from the

ITO/ZnO/PEIE side, the emitted light propagates through more of the chiral F8BT medium, which increases the associated dissymmetry (Table S4).[37] Devices were further optimized by adjusting the thickness of the active layer while keeping the TCTA thickness at 20 nm, which was chosen as the optimal thickness to enhance device performance without affecting the shape of the EL spectrum (Figure S8). The optimized devices demonstrate both high device performance and high g_{EL} (14.5 cd/A, 14.2 lm/W; Figure S9). To the best of our knowledge, these devices represent the first example of CP-OLEDs where there is no longer a trade-off between CP emission and device efficiency.[18–20,37]

To evaluate whether the aza[6]H acts as a PL quencher under 469 nm excitation, we have compared the PLQE of F8BT and F8BT + 10%[*M*] films before and after thermal annealing (Table S6).[36,38] In the case of as-cast films (175 nm), F8BT + 10%[*M*] shows a slightly higher PLQE than neat F8BT (26.5 ± 3.6% *vs*. 22.3 ± 2.8%). After annealing, the PLQE of both films increases to 47.3 ± 4.8% (F8BT + 10%[*M*]) and 38.1 ± 3.1% (neat F8BT), respectively.

In terms of the active layer electronic energy levels, aza[6]H (HOMO = 5.4 eV)[39,40] may act as a hole trap when blended with F8BT (HOMO = 5.8 eV), while its high-lying LUMO level is expected to have negligible impact on the electron mobility.[20] To establish the influence of aza[6]H on charge carrier mobility, we investigated charge transport in conventional single-carrier devices [20]. We found that 10 wt% aza[6]H does not strongly affect the electron current and only slightly reduces the hole current of the active layer.[20] The extraction of charge mobility using analytical expressions such as Mott–Gurney law and its derivatives from space-charge-limited current (SCLC) curves relies on several assumptions, including (1) Ohmic contacts, (2) absence of trap states and (3) negligible voltage drop across interlayers facilitating carrier injection.[41] Thus, we

did not try and extract exact mobility values from the single-carrier measurements due to the inherent uncertainties in this approach (Ref[42] and references therein).

We performed current-voltage measurements on single-carrier iCP-PLED devices with and without the TCTA layer (Figure S10). Without the TCTA hole-transport layer, the hole current density (J_p) is of ~2 orders of magnitude higher than the electron current density (J_n) (J_p/J_n = 52.6, Table S5), which indicates that most holes flow through the device without recombining with electrons. In the high-bias regime the insertion of the TCTA layer decreased the electron current density by a factor of 4, but the hole current density by almost 2 orders of magnitude. We conclude that the TCTA layer not only blocks electrons, but dramatically reduces the flow of holes. This greatly improves the current balance and pushes the RZ towards the blend layer/TCTA interface (J_p/J_n = 4.3, Table S5). By blocking the movement of electrons by the energy step at this interface, TCTA acts to improve the recombination rate while also suppressing non-radiative surface recombination of excitons at the anode. Taken together, these results indicate that the increased PLQE, improved current balance and shifted RZ all played a role in increasing the efficiency of the iCP-OLEDs (Figure S11).

To better understand the vertical composition of the active layer, we made use of surface enhanced Raman spectroscopy (SERS) (Figure S12). By comparing the Raman spectrum (with λ_{ex}= 633 nm) of as-cast and thermally annealed F8BT + 10%[*M*] films deposited on top of (a) bare quartz and (b) a layer of evaporated gold, it is possible to compare the molecular packing in the bulk of the film with that close to the buried interface.[43] This additional sensitivity is achieved because in SERS the Raman vibrational modes of molecules close to a rough gold interface are significantly enhanced. Whilst several of the aza[6]H and F8BT modes overlap (Figure S12), the Raman peak

at 1360 cm^{-1} is dominated by contributions from aza[6]H.[20] Even before the films are annealed, the increase in this mode (1360 cm^{-1}) at the buried interface (on gold) as opposed to the bulk (on quartz) indicates that the aza[6]H molecules tend to migrate to the bottom of the film during the solidification process of thin-film spin coating. The intensity of this peak increases dramatically after annealing, which, combined with the absence of any evidence of aza[6]H in the CD spectra, implies that the aza[6]H phase separates from the polymer active layer during the annealing process.[20]In iCP-PLEDs, the shift of the RZ toward the TCTA/active layer interface, away from the region where in which aza[6]H aggregates, improves device performance.

Figure 3 summarizes possible mechanisms that may explain the improved device performance in iCP-PLEDs. Although F8BT PLEDs usually result in a higher EQE due to their additional singlet exciton formation pathways (i.e. triplet-triplet annihilation and delayed fluorescence), device architecture and carrier balance can also play a role.[44] In conventional (i.e. non-inverted) cCP-PLEDs based on F8BT + 10% aza[6]H,[20] aza[6]H acts as a hole trap as it aggregates close to the hole injection interface. As a result, a high turn-on voltage is required to shift holes from the HOMO of aza[6]H into the deeper HOMO of F8BT.[20] In the iCP-PLEDs without HTLs (TCTA), where hole injection is from the MoO_x/Au side as opposed to the ITO side, holes are directly injected into the F8BT, but trapped by the aza[6]H as they transit towards the ZnO/PEIE. TCTA shifts the RZ away from the ZnO/PEIE, which reduces trapping and non-radiative recombination, and, in turn, enhances excitonic recombination in the highly emissive chiral polymer layer. Without efficiency loss caused by the aza[6]H traps, the optimized devices exhibit excellent performance as previously reported by other groups.[45,46]

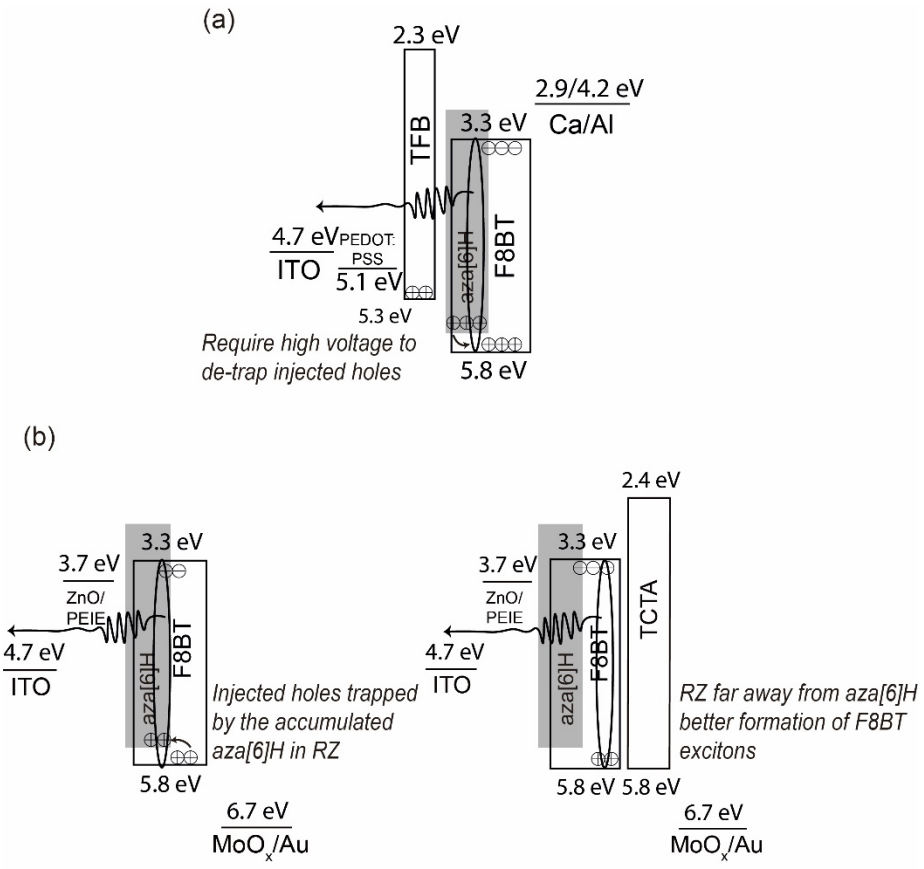

Figure 3. Proposed emission mechanisms for **(a)** cCP-PLED and **(b)** iCP-PLEDs. RZ is shifted by inserting TCTA layer.

Perhaps most remarkably, we find that the chiroptical properties of the CP-PLEDs are sensitive to both the device geometry and active layer thickness (Figures 4 and S13). With a fixed active layer (F8BT + 10% [*P*]-aza[6]H, 150 nm), the cCP-PLED shows a g_{EL} of +0.48, whilst the iCP-PLED shows an *inverted* g_{EL} of –0.37 (with 20 nm TCTA). To explore origins of this intriguing observation, we investigated identical films of F8BT + 10%[*M*] on poly(3,4-ethylenedioxythiophene) polystyrene sulfonate (PEDOT:PSS) and PEIE modified ZnO using CD (Figure S14), Raman (Figure S15), and CP-PL (Figure S16) spectroscopies. We find no evidence of changes in molecular conformation, or the strength of the chiroptical effect, irrespective of the

interlayers used, indicating that ZnO/ PEIE neither alters the active layer morphology nor impacts the mechanism of chiral induction in blend films. As such, these findings suggest that the change in the sign of luminescence dissymmetry depending on device structure may only be occurring due to the electronic generation of excitons.

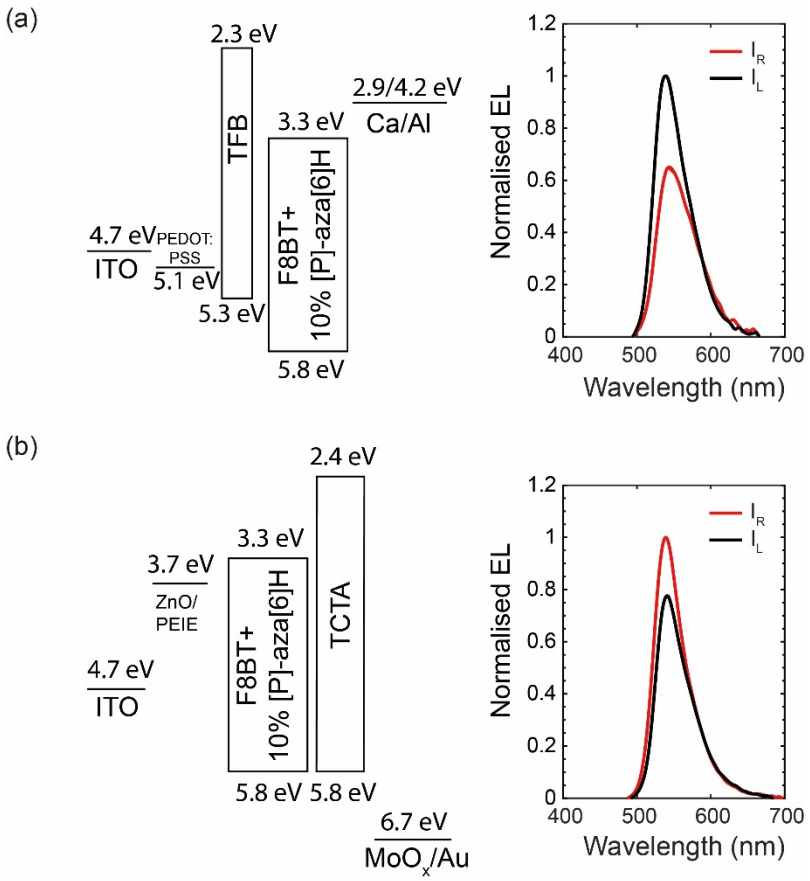

Figure 4. Device architecture and energy level diagrams of **(a)** cCP-PLED and **(b)** iCP-PLED with identical active layer of annealed F8BT + 10%[*P*] (150 nm). All energy levels quoted are prior to layers being stacked altogether, and hence sharing a same vacuum level. Note the opposite handedness of CP-EL.

As the electric field across the emissive layer is in opposite directions in cCP-PLED and iCP-PLEDs, we considered whether the strength and direction of the electric field could impact the

chiroptical effect. To explore this, we performed bias-dependent CP-PL of ITO/F8BT + 10%[*M*]/Au measurements, with the ITO contact held at ground while changing the bias potential at the Au contact. The CP-PL remains the same handedness when the optically excited film is scanned from a negative to a positive bias (Figure S18). Similar to our previous observations for cCP-PLEDs,[20] g_{EL} remains constant in iCP-PLEDs, irrespective of the current density that is applied. This implies that the electric field strength only impacts the luminance of our devices, not the handedness of the emitted light (Figure S17).

Electrically switchable CP-EL is a rarely observed optical phenomenon, and has only been reported in two-dimensional inorganic materials (WSe_2) at ultra-low temperatures (< 40 K)[47]. Otherwise, the generation of opposite handed CP emission has relied on mechanically rotating optical filters or the use of ferromagnetic layers and an external magnetic field. We believe that chiral organic systems, such as the one reported here, may have the potential for the development of electrically switchable CP light emitting devices without demanding experimental requirements (e.g. low temperature, external magnetic field and optics)[48]

This observation of electrically switchable CP-EL emphasizes the need to take the electric field into consideration when analyzing CP-PLEDs and related devices. Whilst it provides a new and unparalleled opportunity to control the handedness of emitted light, elucidation of the precise mechanisms that underpin this observation are beyond the scope of this study. Besides the chiral medium effect that has been discussed previously,[20] spin splitting mechanisms (e.g. Rashba-type[49] / Zeeman-type splitting[50]) might also contribute to the inversion of g_{EL}. These have been demonstrated in previously reported chiral perovskite systems, where imbalanced exciton formation with opposite spin can result in opposite handedness of CP emission.[49,51] Although the classic Rashba-type splitting requires spin-orbit coupling assisted by heavy metal atoms, similar

spin-orbit coupling has been proposed to give rise to the Chirality Induced Spin Selectivity (CISS) effect in several chiral organic systems[52]. Such spin-orbit coupling could then drive a spin splitting effect in our organic system that is similar to the Rashba-type splitting effect.[49] Our study emphasizes the need to develop more sophisticated models to explain CP-EL from cCP-PLEDs, iCP-PLEDs and related devices.

CONCLUSIONS

Through detailed consideration of how to optimize the device performance of our CP blend materials, we have demonstrated highly efficient iCP-OLEDs (typical PE = 16.6 lm/W) with a strong CP emissive dissymmetry (g_{EL} = 0.57). While the chiral small-molecule additive aza[6]H is an efficient, yet simple way to induce strong chiroptical effects in F8BT,[4,20] it is shown to aggregate at the HTL–active layer interface, which may compromise device performance in cCP-OLEDs. The inverted device geometry, and incorporation of a TCTA layer, circumvent this problem, and lead to balanced charge carrier injection, less carrier trapping, which in turn optimizes the location of the recombination zone within the active layer to minimize unfavored non-radiative decay pathways. Additionally, we report an interesting chiroptical phenomenon, where choice of device architecture alone can completely invert the sign of CP-EL. Our approach represents the first demonstration of CP-OLEDs with device performance progressing towards the needs of real-world CP-dependent technologies and applications including highly efficient (CP-) OLED displays.

Experimental Section

Aza[6]H was prepared as previously reported and separated using preparative chiral HPLC.[4]

Solution Preparation and thin film deposition: F8BT (M_w = 31K, Cambridge Display Technology Ltd.) was dissolved with a fixed ratio of aza[6]H (10 wt%) in toluene to form 35 mg/mL solution. Thickness of the thin films was controlled by spin speed (1200–5000 rpm) and measured using a Dektak XT surface profiler.). All annealed samples were annealed for 10 min under nitrogen atmosphere (glovebox, $H_2O < 0.1$ ppm, $O_2 < 0.1$ ppm).

OLED Fabrication and Characterization: Prepatterned ITO substrates were rinsed in an ultrasonic bath with acetone, isopropyl alcohol (IPA) (Sigma Aldrich) and Hellmanex III (Hellma GmbH) and deionized water before deposition of top layers. The ZnO is deposited on the cleaned ITO by a sol-gel method which has been described elsewhere followed by a PEIE (30 wt% in water, Sigma Aldrich) rinsing step. Then, aza[6]helicene blended F8BT was spin-coated onto ZnO/PEIE. Afterwards, TCTA (97% Sigma Aldrich), MoO_x (99.97%, Sigma Aldrich) and Au (99.99%, Kurt J. Lesker Company Ltd.) were thermally evaporated onto the organic layer under vacuum level of ~5×10^{-7} mbar. *J-V-L* characterization (pixel area = 0.045 cm^2) was performed using a Keithley 2400 and Konica Minolta LS-110 Luminance Meter. PLED emission profile was assumed to be Lambertian. EL spectra were measured using an Ocean Optics USB 2000 charge-coupled device spectrophotometer.

Photophysical and Morphological Characterization: Absorption and PL spectra of the blends at various thickness were measured by a Cary 300 UV–Vis spectrometer (Agilent Technologies) and an FLS 1000 (Edinburgh Instruments), respectively. Raman Spectroscopy was performed using a Renishaw inVia Raman microscope, which was calibrated using the silicon Raman band at 520.5 cm^{-1}. The laser spot size was 1 μm^2, and the excitation wavelength was 633 nm for a 20 s accumulation time. PLQE is measured from a FluoroMax 3 fluorospectrometer and analyzed using the method described by Ahn *et al*.[38]

Circular Dichroism, CP-EL and CP-PL: The raw Circular Dichroism data were collected using a Chirascan (Applied Photophysics) instrument. Left-handed and right-handed CP emission spectra from the blended thin films were collected using a linear polarizer and quarter-wave plate prior to an FLS 1000 spectrometer. Both excitation beam and the detector are at a 45 degree to the film and Figure S1 defines CD and CP-PL measurement with different film orientations. The dissymmetry factor g in the CP-PL spectra was calculated from the equation $g = 2(I_L - I_R)/(I_L + I_R)$, $|g| \leq 2$. I_L and I_R are the left-handed and right-handed emission intensities, respectively. A similar method was used to analyze the CP-EL spectra. EL spectra from the PLED were recorded using an Ocean Optics USB 2000 charge-coupled spectrophotometer. All CP-EL measurements are carried out after measuring with only a linear polarizer to ensure negligible linear polarization or random polarization which affects the accuracy of circular polarization measurement.

ASSOCIATED CONTENT

Supporting Information

The Supporting Information is available free of charge on the ACS Publications website. The Supporting Information includes detailed spectroscopy and device data.

AUTHOR INFORMATION

Corresponding Author

* *Matthew J. Fuchter,* m.fuchter@imperial.ac.uk

* *Alasdair J. Campbell,* alasdair.campbell@imperial.ac.uk

Author Contributions

All authors have given approval to the final version of the manuscript.

Funding Sources

This work was supported by EPSRC research grants (EP/P000525/1, EP/L016702/1, EP/R00188X/1).

Conflicts of Interest

A. Campbell and M. Fuchter are inventors on a patent concerning chiral blend materials (WO2014016611).

ACKNOWLEDGMENT

The authors would like to thank Dr. Matthew Roberts and Cambridge Display Technology Limited (Cambridgeshire; Company No. 02672530) for providing the polymers and for their contributions to our understanding of the system. We are grateful to Professor Ji-Seon Kim at Imperial College London for providing access to a Raman spectrometer and Applied Photophysics (Surrey; Company No. 01006739) for their advice on Circular Dichroism measurements.

REFERENCES

(1) Kaji, H.; Suzuki, H.; Fukushima, T.; Shizu, K.; Suzuki, K.; Kubo, S.; Komino, T.; Oiwa, H.; Suzuki, F.; Wakamiya, A.; Murata, Y.; Adachi, C. Purely Organic Electroluminescent Material Realizing 100% Conversion from Electricity to Light. *Nat. Commun.* **2015**, *6* (1), 8476.

(2) Adachi, C.; Baldo, M. A.; Thompson, M. E.; Forrest, S. R. Nearly 100% Internal Phosphorescence Efficiency in an Organic Light-Emitting Device. *J. Appl. Phys.* **2001**, *90* (10), 5048–5051.

(3) Brütting, W.; Frischeisen, J.; Schmidt, T. D.; Scholz, B. J.; Mayr, C. Device Efficiency of Organic Light-Emitting Diodes: Progress by Improved Light Outcoupling. *Phys. status solidi* **2013**, *210* (1), 44–65.

(4) Yang, Y.; Da Costa, R. C.; Smilgies, D. M.; Campbell, A. J.; Fuchter, M. J. Induction of Circularly Polarized Electroluminescence from an Achiral Light-Emitting Polymer via a Chiral Small-Molecule Dopant. *Adv. Mater.* **2013**, *25* (18), 2624–2628.

(5) Brandt, J. R.; Wang, X.; Yang, Y.; Campbell, A. J.; Fuchter, M. J. Circularly Polarized Phosphorescent Electroluminescence with a High Dissymmetry Factor from PHOLEDs Based on a Platinahelicene. *J. Am. Chem. Soc.* **2016**, *138* (31), 9743–9746.

(6) Zinna, F.; Giovanella, U.; Bari, L. Di. Highly Circularly Polarized Electroluminescence from a Chiral Europium Complex. *Adv. Mater.* **2015**, *27* (10), 1791–1795.

(7) Han, J.; Guo, S.; Lu, H.; Liu, S.; Zhao, Q.; Huang, W. Recent Progress on Circularly Polarized Luminescent Materials for Organic Optoelectronic Devices. *Adv. Opt. Mater.* **2018**, *6* (17), 1800538.

(8) Zhang, D.-W.; Li, M.; Chen, C.-F. Recent Advances in Circularly Polarized Electroluminescence Based on Organic Light-Emitting Diodes. *Chem. Soc. Rev.* **2020**, *49* (5), 1331–1343.

(9) Purdie, N.; Swallows, K. A.; Murphy, L. H.; Purdie, R. B. Analytical Applications of Circular Dichroism. *J. Pharm. Biomed. Anal.* **1989**, *7* (12), 1519–1526.

(10) Song, F.; Xu, Z.; Zhang, Q.; Zhao, Z.; Zhang, H.; Zhao, W.; Qiu, Z.; Qi, C.; Zhang, H.; Sung, H. H. Y.; Williams, I. D.; Lam, J. W. Y.; Zhao, Z.; Qin, A.; Ma, D.; Tang, B. Z. Highly Efficient Circularly Polarized Electroluminescence from Aggregation-Induced

Emission Luminogens with Amplified Chirality and Delayed Fluorescence. *Adv. Funct. Mater.* **2018**, *28* (17), 1800051.

(11) Imagawa, T.; Hirata, S.; Totani, K.; Watanabe, T.; Vacha, M. Thermally Activated Delayed Fluorescence with Circularly Polarized Luminescence Characteristics. *Chem. Commun.* **2015**, *51* (68), 13268–13271.

(12) Yan, Z.; Luo, X.; Liu, W.; Wu, Z.; Liang, X.; Liao, K.; Wang, Y.; Zheng, Y.; Zhou, L.; Zuo, J.; Pan, Y.; Zhang, H. Configurationally Stable Platinahelicene Enantiomers for Efficient Circularly Polarized Phosphorescent Organic Light-Emitting Diodes. *Chem. Eur. J.* **2019**, *25* (22), 5672–5676.

(13) Wu, Z.; Han, H.; Yan, Z.; Luo, X.; Wang, Y.; Zheng, Y.; Zuo, J.; Pan, Y. Chiral Octahydro-Binaphthol Compound-Based Thermally Activated Delayed Fluorescence Materials for Circularly Polarized Electroluminescence with Superior EQE of 32.6% and Extremely Low Efficiency Roll-Off. *Adv. Mater.* **2019**, *31* (28), 1900524.

(14) Li, M.; Li, S.-H.; Zhang, D.; Cai, M.; Duan, L.; Fung, M.-K.; Chen, C.-F. Stable Enantiomers Displaying Thermally Activated Delayed Fluorescence: Efficient OLEDs with Circularly Polarized Electroluminescence. *Angew. Chemie Int. Ed.* **2018**, *57* (11), 2889–2893.

(15) Li, M.; Wang, Y.; Zhang, D.; Duan, L.; Chen, C. Axially Chiral TADF-Active Enantiomers Designed for Efficient Blue Circularly Polarized Electroluminescence. *Angew. Chemie Int. Ed.* **2020**, *59* (9), 3500–3504.

(16) Yang, Y.; da Costa, R. C.; Fuchter, M. J.; Campbell, A. J. Circularly Polarized Light Detection by a Chiral Organic Semiconductor Transistor. *Nat. Photonics* **2013**, *7* (8), 634–638.

(17) Lakhwani, G.; Meskers, S. C. J. Insights from Chiral Polyfluorene on the Unification of Molecular Exciton and Cholesteric Liquid Crystal Theories for Chiroptical Phenomena. *J. Phys. Chem. A* **2012**, *116* (4), 1121–1128.

(18) Di Nuzzo, D.; Kulkarni, C.; Zhao, B.; Smolinsky, E.; Tassinari, F.; Meskers, S. C. J.; Naaman, R.; Meijer, E. W.; Friend, R. H. High Circular Polarization of Electroluminescence Achieved via Self-Assembly of a Light-Emitting Chiral Conjugated Polymer into Multidomain Cholesteric Films. *ACS Nano* **2017**, *11* (12), 12713–12722.

(19) Lee, D.-M.; Song, J.-W.; Lee, Y.-J.; Yu, C.-J.; Kim, J.-H. Control of Circularly Polarized Electroluminescence in Induced Twist Structure of Conjugate Polymer. *Adv. Mater.* **2017**, *29* (29), 1700907.

(20) Wan, L.; Wade, J.; Salerno, F.; Arteaga, O.; Laidlaw, B.; Wang, X.; Penfold, T.; Fuchter, M. J.; Campbell, A. J. Inverting the Handedness of Circularly Polarized Luminescence from Light-Emitting Polymers Using Film Thickness. *ACS Nano* **2019**, *13* (7), 8099–8105.

(21) Peeters, E.; Christiaans, M. P. T.; Janssen, R. A. J.; Schoo, H. F. M.; Dekkers, H. P. J. M.; Meijer, E. W. Circularly Polarized Electroluminescence from a Polymer Light-Emitting Diode. *J. Am. Chem. Soc.* **1997**, *119* (41), 9909–9910.

(22) Oda, M.; Nothofer, H.-G.; Lieser, G.; Scherf, U.; Meskers, S. C. J.; Neher, D. Circularly Polarized Electroluminescence from Liquid-Crystalline Chiral Polyfluorenes. *Adv. Mater.* **2000**, *12* (5), 362–365.

(23) Liu, Z.-T.; Huang, Y.-Y.; Li, Y.; He, Y.-M.; Fan, Q.-H. Synthesis and Chiroptical Properties of Chiral Binaphthyl-Containing Polyfluorene Derivatives. *J. Polym. Sci. Part A Polym. Chem.* **2011**, *49* (3), 680–689.

(24) Lee, B. R.; Jung, E. D.; Park, J. S.; Nam, Y. S.; Min, S. H.; Kim, B.-S.; Lee, K.-M.; Jeong, J.-R.; Friend, R. H.; Kim, J.-S.; Kim, S. O.; Song, M. H. Highly Efficient Inverted Polymer Light-Emitting Diodes Using Surface Modifications of ZnO Layer. *Nat. Commun.* **2014**, *5* (1), 4840.

(25) Kabra, D.; Lu, L. P.; Song, M. H.; Snaith, H. J.; Friend, R. H. Efficient Single-Layer Polymer Light-Emitting Diodes. *Adv. Mater.* **2010**, *22* (29), 3194–3198.

(26) Suh, M.; Bailey, J.; Kim, S. W.; Kim, K.; Yun, D.-J.; Jung, Y.; Hamilton, I.; Chander, N.; Wang, X.; Bradley, D. D. C.; Jeon, D. Y.; Kim, J.-S. High-Efficiency Polymer LEDs with Fast Response Times Fabricated via Selection of Electron-Injecting Conjugated Polyelectrolyte Backbone Structure. *ACS Appl. Mater. Interfaces* **2015**, *7* (48), 26566–26571.

(27) Kim, Y.-H.; Han, T.-H.; Cho, H.; Min, S.-Y.; Lee, C.-L.; Lee, T.-W. Polyethylene Imine as an Ideal Interlayer for Highly Efficient Inverted Polymer Light-Emitting Diodes. *Adv. Funct. Mater.* **2014**, *24* (24), 3808–3814.

(28) Fukagawa, H. Molecular Design and Device Design to Improve Stabilities of Organic Light-Emitting Diodes. *J. Photopolym. Sci. Technol.* **2018**, *31* (3), 315–321.

(29) Kim, J.; Kim, H.-M.; Jang, J. Low Work Function 2.81 EV Rb 2 CO 3 -Doped Polyethylenimine Ethoxylated for Inverted Organic Light-Emitting Diodes. *ACS Appl. Mater. Interfaces* **2018**, *10* (22), 18993–19001.

(30) Vacek Chocholoušová, J.; Vacek, J.; Andronova, A.; Míšek, J.; Songis, O.; Šámal, M.; Stará, I. G.; Meyer, M.; Bourdillon, M.; Pospíšil, L.; Starý, I. On the Physicochemical Properties of Pyridohelicenes. *Chem. Eur. J.* **2014**, *20* (3), 877–893.

(31) Albano, G.; Górecki, M.; Pescitelli, G.; Di Bari, L.; Jávorfi, T.; Hussain, R.; Siligardi, G. Electronic Circular Dichroism Imaging (CD *i*) Maps Local Aggregation Modes in Thin Films of Chiral Oligothiophenes. *New J. Chem.* **2019**, *43* (36), 14584–14593.

(32) Cui, X.; Nichols, S. M.; Arteaga, O.; Freudenthal, J.; Paula, F.; Shtukenberg, A. G.; Kahr, B. Dichroism in Helicoidal Crystals. *J. Am. Chem. Soc.* **2016**, *138* (37), 12211–12218.

(33) Jhulki, S.; Moorthy, J. N. Small Molecular Hole-Transporting Materials (HTMs) in Organic Light-Emitting Diodes (OLEDs): Structural Diversity and Classification. *J. Mater. Chem. C* **2018**, *6* (31), 8280–8325.

(34) Faria, J. C. D.; Campbell, A. J.; McLachlan, M. A. Fluorene Copolymer Bilayers for Emission Colour Tuning in Inverted Hybrid Light Emitting Diodes. *J. Mater. Chem. C* **2015**, *3* (19), 4945–4953.

(35) Craig, M. R.; Jonkheijm, P.; Meskers, S. C. J.; Schenning, A. P. H. J.; Meijer, E. W. The Chiroptical Properties of a Thermally Annealed Film of Chiral Substituted Polyfluorene Depend on Film Thickness. *Adv. Mater.* **2003**, *15* (17), 1435–1438.

(36) Donley, C. L.; Zaumseil, J.; Andreasen, J. W.; Nielsen, M. M.; Sirringhaus, H.; Friend, R. H.; Kim, J.-S. Effects of Packing Structure on the Optoelectronic and Charge Transport Properties in Poly(9,9-Di- n -Octylfluorene- Alt -Benzothiadiazole). *J. Am. Chem. Soc.* **2005**, *127* (37), 12890–12899.

(37) Jung, J.-H.; Lee, D.; Kim, J.-H.; Yu, C. Circularly Polarized Electroluminescence by Controlling the Emission Zone in a Twisted Mesogenic Conjugate Polymer. *J. Mater. Chem. C* **2018**, *6* (4), 726–730.

(38) Ahn, T.; Al-Kaysi, R. O.; Müller, A. M.; Wentz, K. M.; Bardeen, C. J. Self-Absorption Correction for Solid-State Photoluminescence Quantum Yields Obtained from Integrating Sphere Measurements. *Rev. Sci. Instrum.* **2007**, *78* (8), 086105.

(39) Weimar, M.; Correa da Costa, R.; Lee, F.-H.; Fuchter, M. J. A Scalable and Expedient Route to 1-Aza[6]Helicene Derivatives and Its Subsequent Application to a Chiral-Relay Asymmetric Strategy. *Org. Lett.* **2013**, *15* (7), 1706–1709.

(40) Salerno, F.; Rice, B.; Schmidt, J. A.; Fuchter, M. J.; Nelson, J.; Jelfs, K. E. The Influence of Nitrogen Position on Charge Carrier Mobility in Enantiopure Aza[6]Helicene Crystals. *Phys. Chem. Chem. Phys.* **2019**, *21* (9), 5059–5067.

(41) Shi, X.; Nádaždy, V.; Perevedentsev, A.; Frost, J. M.; Wang, X.; Von Hauff, E.; Mackenzie, R. C. I.; Nelson, J. Relating Chain Conformation to the Density of States and Charge Transport in Conjugated Polymers: The Role of the β-Phase in Poly(9,9-Dioctylfluorene). *Phys. Rev. X* **2019**, *9* (2), 021038.

(42) Harding, M. J.; Poplavskyy, D.; Choong, V.-E.; So, F.; Campbell, A. J. Variations in Hole Injection Due to Fast and Slow Interfacial Traps in Polymer Light-Emitting Diodes with Interlayers. *Adv. Funct. Mater.* **2010**, *20* (1), 119–130.

(43) Félidj, N.; Aubard, J.; Lévi, G.; Krenn, J. R.; Hohenau, A.; Schider, G.; Leitner, A.; Aussenegg, F. R. Optimized Surface-Enhanced Raman Scattering on Gold Nanoparticle Arrays. *Appl. Phys. Lett.* **2003**, *82* (18), 3095–3097.

(44) Dey, A.; Chandrasekaran, N.; Chakraborty, D.; Johari, P.; McNeill, C. R.; Rao, A.; Kabra, D. Kinetics of Thermally Activated Triplet Fusion as a Function of Polymer Chain Packing in Boosting the Efficiency of Organic Light Emitting Diodes. *npj Flex. Electron.* **2018**, *2* (1), 28.

(45) Lu, L. P.; Kabra, D.; Friend, R. H. Barium Hydroxide as an Interlayer Between Zinc Oxide and a Luminescent Conjugated Polymer for Light-Emitting Diodes. *Adv. Funct. Mater.* **2012**, *22* (19), 4165–4171.

(46) Dey, A.; Rao, A.; Kabra, D. A Complete Quantitative Analysis of Spatio-Temporal Dynamics of Excitons in Functional Organic Light-Emitting Diodes. *Adv. Opt. Mater.* **2017**, *5* (2), 1600678.

(47) Zhang, Y. J.; Oka, T.; Suzuki, R.; Ye, J. T.; Iwasa, Y. Electrically Switchable Chiral Light-Emitting Transistor. *Science* **2014**, *344* (6185), 725–728.

(48) Zaumseil, J. Electronic Control of Circularly Polarized Light Emission. *Science* **2014**, *344* (6185), 702–703.

(49) Niesner, D.; Wilhelm, M.; Levchuk, I.; Osvet, A.; Shrestha, S.; Batentschuk, M.; Brabec, C.; Fauster, T. Giant Rashba Splitting in $CH_3NH_3PbBr_3$ Organic-Inorganic Perovskite. *Phys. Rev. Lett.* **2016**, *117* (12), 126401.

(50) Singh, R.; Narayanan Unni, K. N.; Solanki, A.; Deepak. Improving the Contrast Ratio of OLED Displays: An Analysis of Various Techniques. *Opt. Mater.* **2012**, *34* (4), 716–723.

(51) Long, G.; Jiang, C.; Sabatini, R.; Yang, Z.; Wei, M.; Quan, L. N.; Liang, Q.; Rasmita, A.; Askerka, M.; Walters, G.; Gong, X.; Xing, J.; Wen, X.; Quintero-Bermudez, R.; Yuan, H.; Xing, G.; Wang, X. R.; Song, D.; Voznyy, O.; Zhang, M.; Hoogland, S.; Gao, W.; Xiong, Q.; Sargent, E. H. Spin Control in Reduced-Dimensional Chiral Perovskites. *Nat. Photonics* **2018**, *12* (9), 528–533.

(52) Naaman, R.; Waldeck, D. H. Chiral-Induced Spin Selectivity Effect. *J. Phys. Chem. Lett.* **2012**, *3* (16), 2178–2187.